SUPPLEMENTAL INFORMATION

Inhibition of Pro-Apoptotic BAX by a Noncanonical Interaction Mechanism

Lauren A. Barclay, Thomas E. Wales, Thomas P. Garner, Franziska Wachter, Susan Lee, Rachel Guerra, Michelle L. Stewart, Craig R. Braun, Gregory H. Bird, Evripidis Gavathiotis, John R. Engen, and Loren D. Walensky

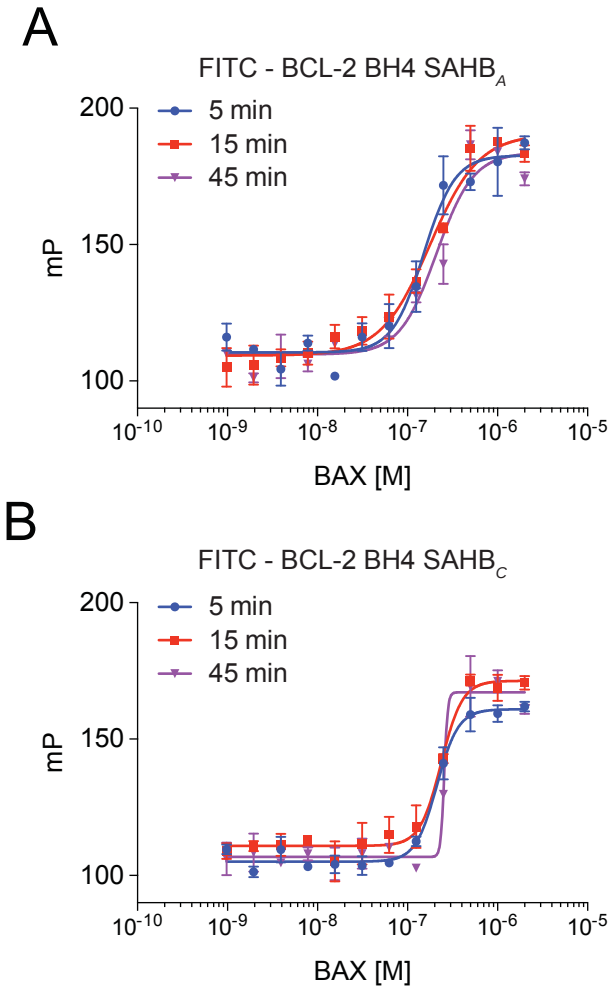

Figure S1, related to Figure 1

Figure S1, related to Figure 1

BCL-2 BH4 SAHBs *A* and *C* Directly Bind to Pro-Apoptotic BAX

(A, B) FITC-BCL-2 BH4 $SAHB_A$ and FITC-BCL-2 BH4 $SAHB_C$ stably bind to recombinant, full-length BAX with nanomolar affinity (e.g. $EC_{50s,}$ 177 nM and 236 nM, respectively, at 15 min), as demonstrated by fluorescence polarization assay monitored over time. Data are mean $\pm$ SD for experiments performed in duplicate.

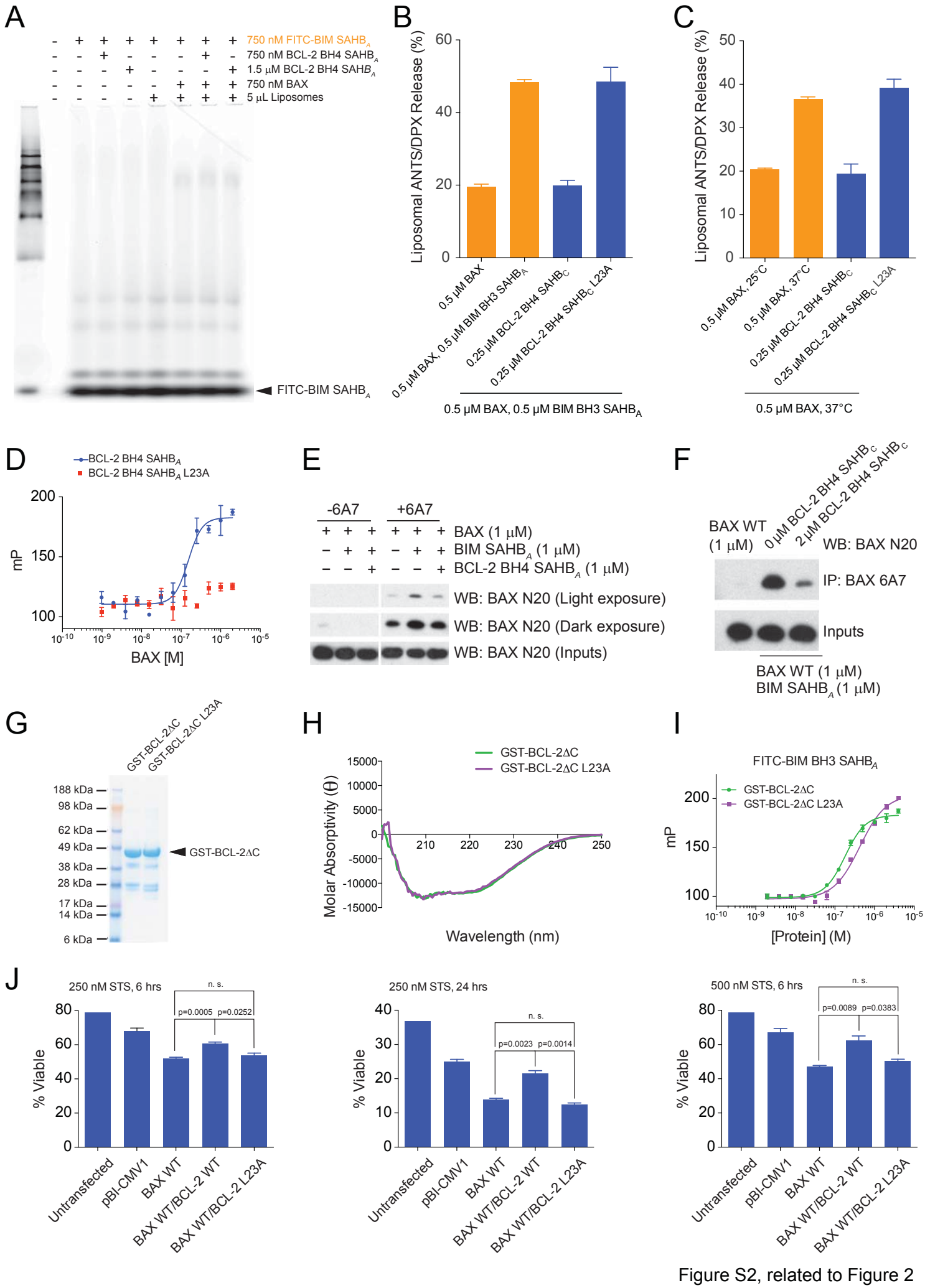

Figure S2, related to Figure 2

Figure S2, related to Figure 2

Biochemical and Cellular Activities of BCL-2 BH4 SAHBs, BCL-2 Proteins, and their L23A Mutant Forms

(A) Native gel electrophoresis and FITC scan analysis of FITC-BIM $SAHB_A$ in the presence and absence of BCL-2 BH4 $SAHB_A$, liposomes, and wild-type BAX.

(B, C) BCL-2 BH4 $SAHB_C$, but not BCL-2 BH4 $SAHB_C$ L23A, inhibits BIM $SAHB_A$-triggered (B) and heat-induced (C) BAX activation, as measured by liposomal release assay. Data are mean ± SD for experiments performed in triplicate.

(D) FITC-BCL-2 BH4 $SAHB_A$, but not the L23A mutant, stably engages BAX, as measured by fluorescence polarization assay. Data are mean ± SD for experiments performed in duplicate.

(E) Treatment of BAX with BIM $SAHB_A$ promotes 6A7 epitope exposure, whereas co-treatment with BCL-2 BH4 $SAHB_A$ suppresses the effect. This control experiment demonstrates that pull-down of activated BAX from the liposomal preparation is dependent upon the presence of the 6A7 antibody.

(F) Like BCL-2 BH4 $SAHB_A$, BCL-2 BH4 $SAHB_C$ impairs the conformational activation of BAX by BIM $SAHB_A$, as monitored by 6A7 immunoprecipitation assay.

(G) Gel electrophoresis and Coomassie stain of recombinant GST-BCL-2ΔC and GST-BCL-2ΔC L23A (M.W. ~50 kDa).

(H) L23A point mutagenesis of GST-BCL-2ΔC does not affect the overall protein fold, as documented by circular dichroism analysis that demonstrates identical spectra for GST-BCL-2ΔC and GST-BCL-2ΔC L23A.

(I) The L23A mutant form of GST-BCL-2ΔC retains BIM $SAHB_A$ binding activity, as measured by fluorescence polarization assay, indicating that the canonical BH3-binding pocket is functionally intact in GST-BCL-2ΔC L23A. Data are mean ± SD for assays performed in duplicate.

(J) L23A mutagenesis reduced the capacity of BCL-2 to protect against apoptosis of HeLa cells co-expressing full-length BAX and BCL-2, and induced with staurosporine at the indicated doses and durations. Data are mean ± SD for experiments performed in triplicate.

A

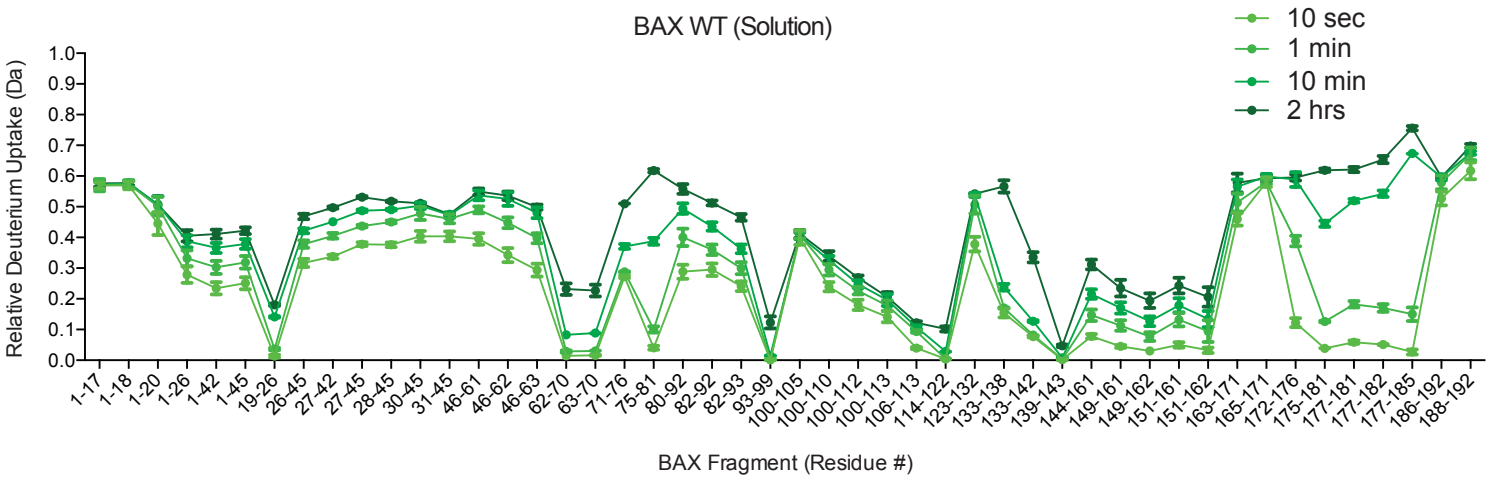

B

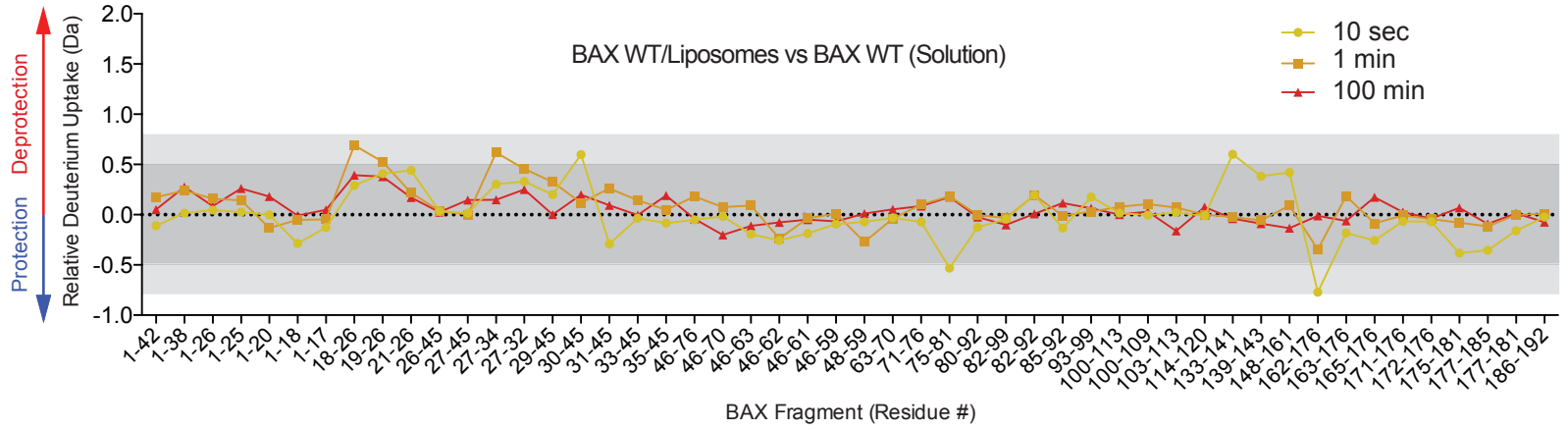

Figure S3, related to Figures 3 and 4

Figure S3, related to Figures 3 and 4

Deuterium Exchange Profiles of Wild-Type BAX in Solution and in the Presence of Liposomes

(A) The deuterium exchange profile of wild-type BAX in solution, incubated at room temperature for 10 sec, 1 min, 10 min, and 2 hr, reveals a range of deuterium uptake across the protein sequence reflecting the differences in flexibility and solvent exposure across discrete regions of BAX.

(B) The relative difference in deuterium exchange between full-length BAX in the presence and absence of liposomes was determined following 10 sec (yellow), 1 min (orange), and 100 min (red) of deuterium exposure. Incubation with liposomes had little to no effect on deuterium uptake by BAX. Dark grey shading represents changes in the plot that are below the significance threshold of 0.5 Da, whereas light grey shading and the white region highlight changes above the baseline significance threshold of 0.5 Da and the even more stringent threshold of 0.8 Da, respectively.

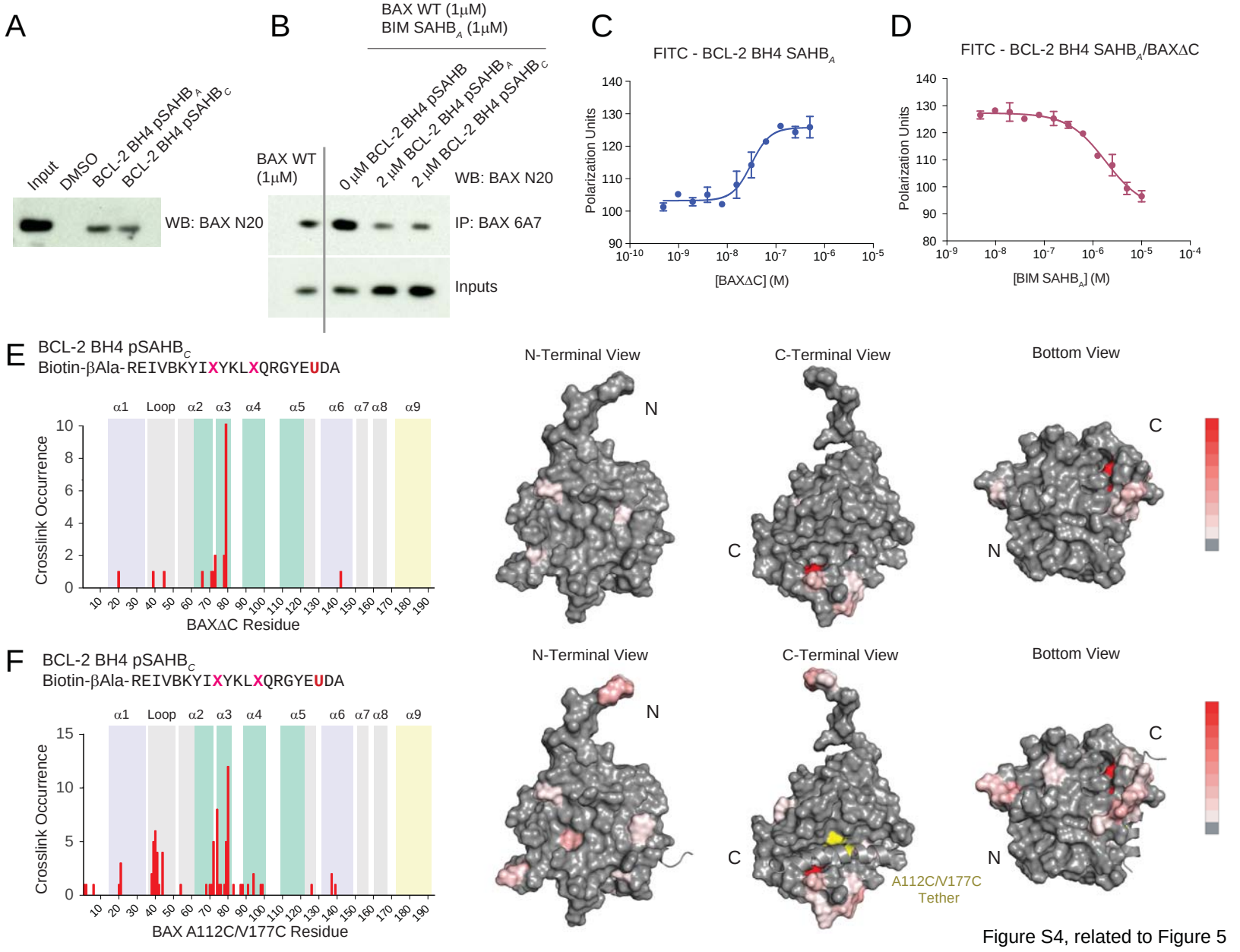

Figure S4, related to Figure 5

Figure S4, related to Figure 5

BAX Binding and Photo-crosslinking Activities of BCL-2 BH4 SAHBs

(A) Biotinylated BCL-2 BH4 pSAHBs *A* and *C* bind to native BAX from HeLa cell lysates, as assessed by streptavadin pull-down.

(B) Both BCL-2 BH4 pSAHBs *A* and *C* suppress the conformational activation of BAX by BIM $SAHB_A$, as assessed by 6A7 immunoprecipitation of recombinant BAX treated in the presence of liposomes.

(C) Fluorescence polarization binding analysis demonstrated that FITC-BCL-2 BH4 $SAHB_A$ bound to BAXΔC with low nanomolar affinity (EC_{50}, 31 nM).

(D) The direct activator ligand, BIM $SAHB_A$ (aa 145-164), dose-responsively competed with FITC BCL-2 BH4 $SAHB_A$ for BAXΔC engagement (IC_{50} of 1.8 μM). Data are mean ± SD for assays performed in duplicate and repeated at least twice.

(E, D) Photoaffinity labeling of BAXΔC and α9-tethered BAX A112C/V177C by BCL-2 BH4 $SAHB_C$ revealed similar crosslinking patterns when compared to each other and full-length BAX (Figure 5B). These data indicated that C-terminal pocket exposure by α9 deletion or covalent reinforcement of α9 engagement to block the C-terminal pocket do not significantly alter the binding and crosslinking activity of BCL-2 BH4 $pSAHB_C$. The plots (left) depict the frequency of crosslinked sites identified across the BAXΔC and BAX A112C/V177C polypeptide sequences with the crosslinked residues mapped onto the solution structure of monomeric BAX (PDB: 1F16) (right) and colored according to the frequency of occurrence. The site of the α5-α9 tether in BAX A112C/V177C is colored yellow.

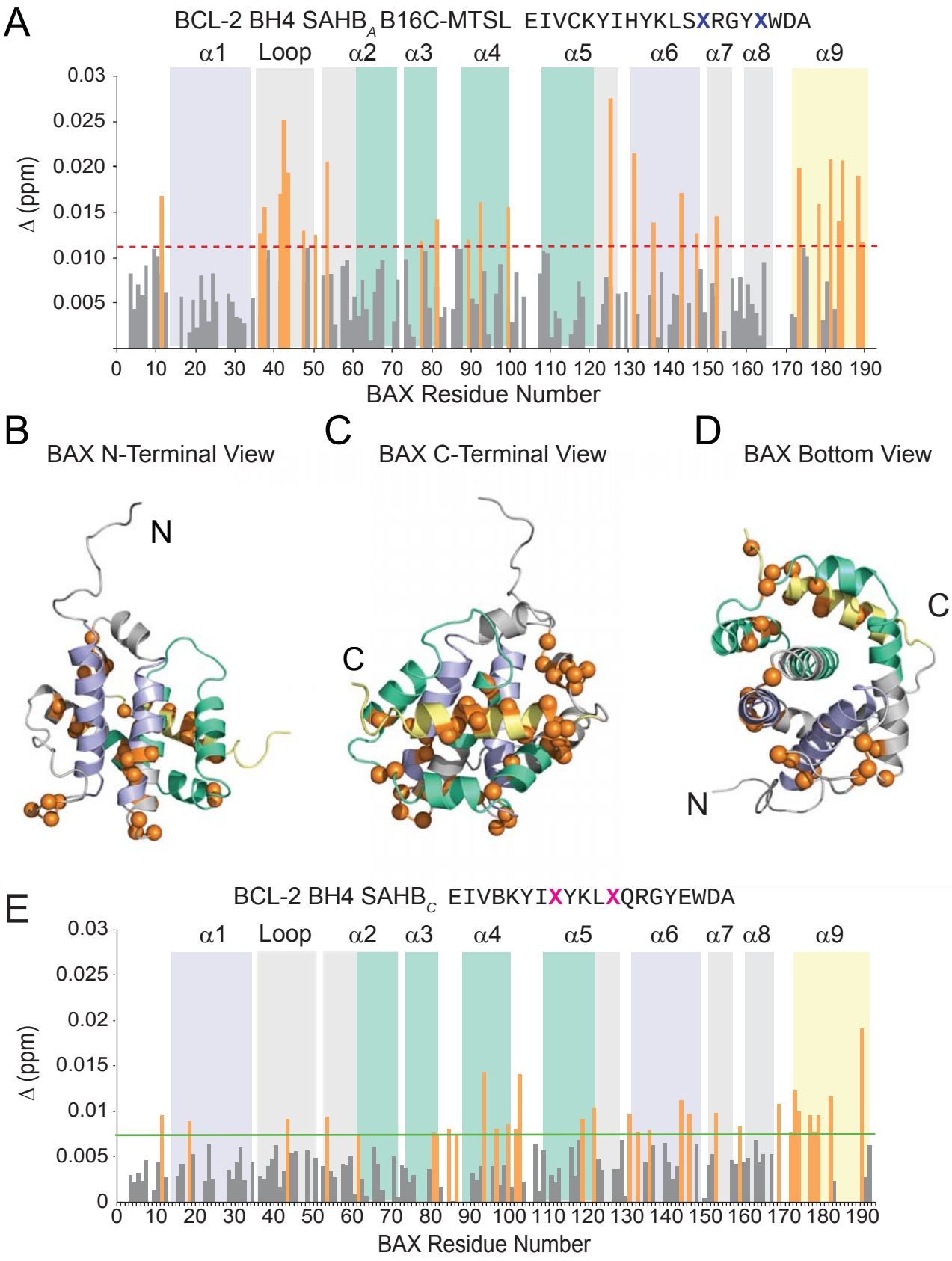

Figure S5, related to Figure 6

Figure S5, related to Figure 6

HSQC NMR analyses of BAX upon Titration with BCL-2 BH4 SAHBs

(A-D) NMR analysis of ^{15}N-BAX upon titration with BCL-2 BH4 SAHB$_A$ B16C-MTSL$_{ox}$ demonstrated a similar pattern of chemical shift changes as observed for BCL-2 BH4 SAHB$_A$ Y28C-MTSL (Figure 6A), with residues of the α1-α2 loop, α3-α4 and α5-α6 hairpins, and α9 notably affected. Cα atoms of affected residues are represented as orange bars in the plot (A) and orange spheres in the ribbon diagrams (B-D). The significance threshold of >0.017 p.p.m. for backbone amide chemical shift changes was calculated based on the average chemical shift across all residues plus the standard deviation, as previously reported(Gavathiotis et al., 2008) and in accordance with standard methods(Marintchev et al., 2007). The α1/α6 region that comprises the N-terminal trigger site is colored magenta, those portions of α-helices 2, 3, 4, and 5 that contain residues forming the C-terminal canonical groove are colored green, and the C-terminal α9 helix is colored yellow.

(E) The NMR analysis was repeated with BCL-2 BH4 SAHB$_c$, an alternate BH4 SAHB lacking C-MTSL substitution and bearing the *C* rather than *A* staple position. Although the observed chemical shift changes were weaker for this construct (significance threshold of >0.007), a similar pattern of affected residues was observed when compared to the MTSL-labeled BCL-2 BH4 SAHB$_A$ constructs (Figures 6A and S5A).

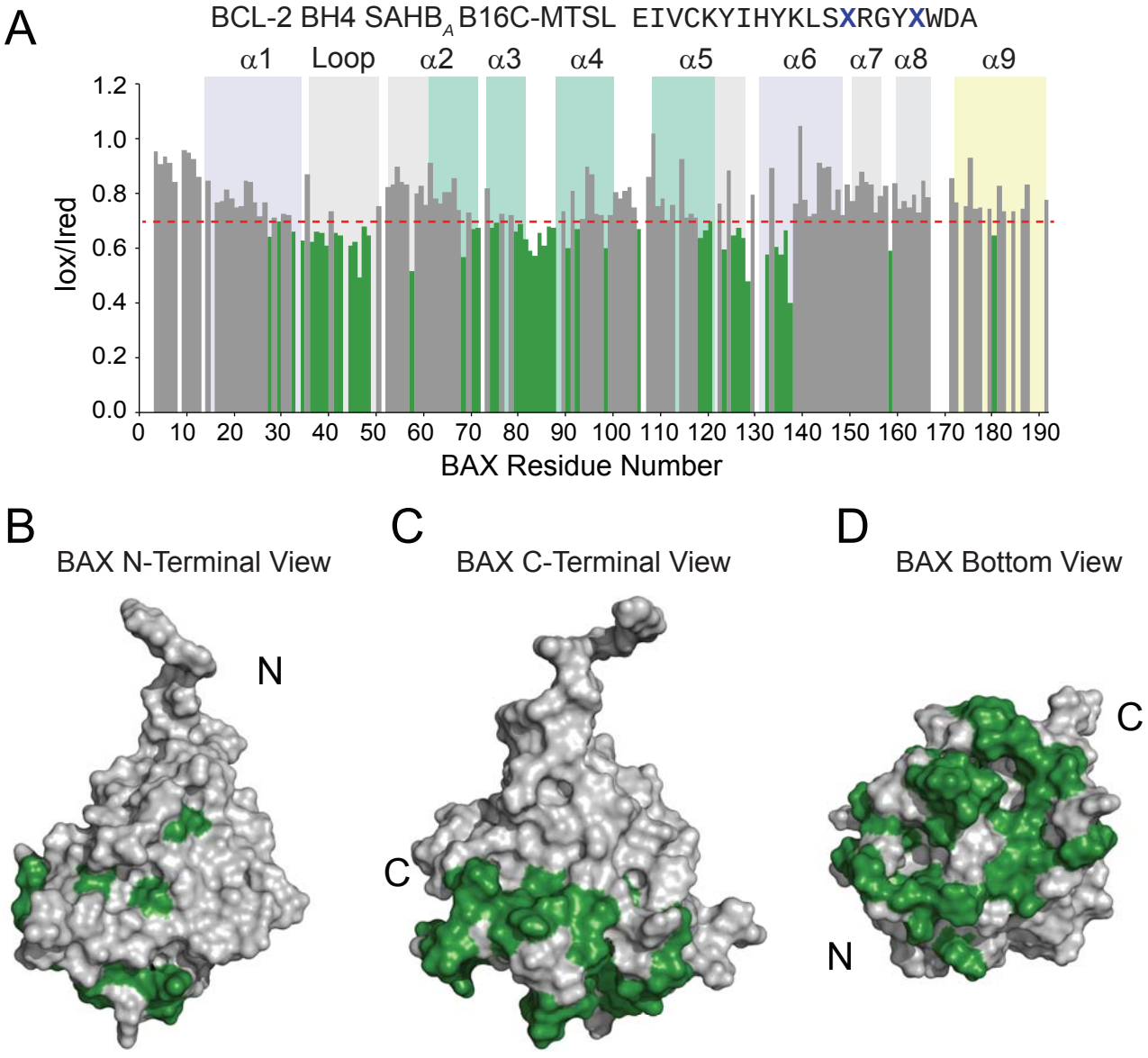

Figure S6, related to Figure 6

Figure S6, related to Figure 6

PRE NMR analyses of the BCL-2 BH4 SAHB$_A$/BAX Interaction
(A-D) Ratios of BAX cross-peak intensities in the presence of oxidized or reduced (I_{ox}/I_{red}) BCL-2 BH4 SAHB$_A$ B16C-MTSL plotted versus BAX residue number. BAX residue intensities reduced below a ratio of 0.7 are colored green in the plot (A) and mapped onto surface views of the BAX structure (B-D). BAX residues affected by the MTSL label colocalize to the bottom face of BAX in a region spanning from the base of the C-terminal pocket to the α1-α2 loop of the N-terminal face.

Stapled BH4 and BH3 Peptide Compositions

Peptide	Sequence	N-terminus	Figures
BCL-2 BH4 SAHB$_A$	**EIVBKYIHYKLSXRGYXWDA**	Acetyl, FITC-βAla, Btn-βAla	1,2,3,4,S1,S2,S4
BCL-2 BH4 SAHB$_B$	**EIVBKYIHXKLSXRGYEWDA**	Acetyl	1
BCL-2 BH4 SAHB$_C$	**EIVBKYIXYKLXQRGYEWDA**	Acetyl, FITC-βAla	1,S1,S2,S5
BCL-2 BH4 SAHB$_D$	**EIVBKYXHYKXSQRGYEWDA**	Acetyl	1
BCL-2 BH4 SAHB$_A$ E13A	**AIVBKYIHYKLSXRGYXWDA**	FITC-βAla	2
BCL-2 BH4 SAHB$_A$ I14A	**EAVBKYIHYKLSXRGYXWDA**	FITC-βAla	2
BCL-2 BH4 SAHB$_A$ V15A	**EIABKYIHYKLSXRGYXWDA**	FITC-βAla	2
BCL-2 BH4 SAHB$_A$ B16A	**EIVAKYIHYKLSXRGYXWDA**	FITC-βAla	2
BCL-2 BH4 SAHB$_A$ K17A	**EIVBAYIHYKLSXRGYXWDA**	FITC-βAla	2
BCL-2 BH4 SAHB$_A$ Y18A	**EIVBKAIHYKLSXRGYXWDA**	FITC-βAla	2
BCL-2 BH4 SAHB$_A$ I19A	**EIVBKYAHYKLSXRGYXWDA**	FITC-βAla	2
BCL-2 BH4 SAHB$_A$ H20A	**EIVBKYIAYKLSXRGYXWDA**	FITC-βAla	2
BCL-2 BH4 SAHB$_A$ Y21A	**EIVBKYIHAKLSXRGYXWDA**	FITC-βAla	2
BCL-2 BH4 SAHB$_A$ K22A	**EIVBKYIHYALSXRGYXWDA**	FITC-βAla	2
BCL-2 BH4 SAHB$_A$ L23A	**EIVBKYIHYKASXRGYXWDA**	Acetyl, FITC-βAla, Btn-βAla	2,3,4,S2
BCL-2 BH4 SAHB$_A$ S24A	**EIVBKYIHYKLAXRGYXWDA**	FITC-βAla	2
BCL-2 BH4 SAHB$_A$ R26A	**EIVBKYIHYKLSXAGYXWDA**	FITC-βAla	2
BCL-2 BH4 SAHB$_A$ G27A	**EIVBKYIHYKLSXRAYXWDA**	FITC-βAla	2
BCL-2 BH4 SAHB$_A$ G27E	**EIVBKYIHYKLSXREYXWDA**	FITC-βAla	2
BCL-2 BH4 SAHB$_A$ Y28A	**EIVBKYIHYKLSXRGAXWDA**	FITC-βAla	2
BCL-2 BH4 SAHB$_A$ W30A	**EIVBKYIHYKLSXRGYXADA**	FITC-βAla	2
BCL-2 BH4 SAHB$_A$ D31A	**EIVBKYIHYKLSXRGYXWAA**	FITC-βAla	2
BCL-2 BH4 SAHB$_A$ A32E	**EIVBKYIHYKLSXRGYXWDE**	FITC-βAla	2
BCL-2 BH4 SAHB$_C$ L23A	**EIVBKYIXYKAXQRGYEWDA**	FITC-βAla	S2
BCL-2 BH4 pSAHB$_A$	**EIVBKYUHYKLSXRGYXWDA**	Btn-βAla	5,S4
BCL-2 BH4 pSAHB$_C$	**EIVBKYIXYKLXQRGYEUDA**	Btn-βAla	5,S4
BCL-2 BH4 SAHB$_A$ B16C-MTSL	**EIVCKYIHYKLSXRGYXWDA**	Acetyl	7,S5,S6
BCL-2 BH4 SAHB$_A$ Y28C-MTSL	**EIVBKYIHYKLSXRGCXWDA**	Acetyl	6,7,S6
BIM BH3 SAHB$_A$	**EIWIAQELRXIGDXFNAYYA**	Acetyl, FITC-βAla	2,4,S2

X, stapling amino acid; B, norleucine; U, 4-benzoyl-phenylalanine (Bpa)

Table S1, related to Figures 1-7

Table S1, related to Figures 1-7

Stapled BH4 and BH3 Peptide Compositions

Supplemental Experimental Procedures

Recombinant BCL-2 Protein Expression and Purification

GST-BCL-2ΔC L23A was generated by site-directed mutagenesis of the pGEX-4t1 vector and confirmed by DNA sequencing. GST-BCL-2ΔC constructs were expressed in E. coli by inducing with 100 mM isopropyl β-D-1-thiogalactopyranoside (IPTG). The bacterial pellet was resuspended in lysis buffer (1% Triton in PBS), sonicated, and ultracentrifuged at 45,000xg for 45 min. The supernatant was applied to pre-equilibrated glutathione sepharose (GE Healthcare) and washed with 1% Triton in PBS followed by additional PBS washes. GST-tagged protein was eluted by six successive washes with elution buffer (10 mM reduced glutathione [Sigma], 50 mM Tris-HCl, pH 8.0) for 10 min at room temperature. Excess glutathione was removed by overnight dialysis into the corresponding assay buffer.

Circular Dichroism

CD spectra of GST-BCL-2ΔC constructs (9 μM) in assay buffer (5 mM potassium phosphate, pH 7.4) were obtained using an Aviv Biomedical spectrometer (Model 410) at 20°C. Molar absorptivity (θ) was calculated as described(Bird et al., 2008).

Fluorescence Polarization Binding Analysis

Fluoresceinated (FITC)-peptide (50 nM) was incubated with recombinant full length BAX, BAXΔC, or GST-BCL-2ΔC proteins at the indicated concentrations in NMR buffer (50 mM NaCl, 20 mM potassium phosphate, pH 6.0), binding buffer (140 mM NaCl, 50 mM Tris-HCl, pH 7.4), or binding buffer optimized for anti-apoptotic proteins (100 mM NaCl, 50 mM Tris-HCl, pH 8.0), respectively, at room temperature. For competition assays, a serial dilution of N-terminal acetylated peptide was incubated with a fixed concentration of FITC-peptide and BAXΔC (50 nM and 125 nM, respectively). Fluorescence polarization was measured at the indicated time points using a SpectraMax M5 microplate reader. EC_{50} and IC_{50} values were determined by nonlinear regression analysis of dose-response curves using Prism software 4.0 (GraphPad).

Peptide Association Assay

FITC-BIM BH3 $SAHB_A$ was incubated in liposomal assay buffer in the presence or absence of the indicated amounts of acetylated BCL-2 BH4 $SAHB_A$, liposomes, and recombinant full-length BAX in a total volume of 30 μL. Following incubation at room temperature for 60 min, samples were resolved by native gel electrophoresis using an 18% Tris-Glycine gel (Novagen) and visualized by fluorescence imaging (Typhoon 9400, GE Healthcare).

Solution-phase Hydrogen/Deuterium Exchange Mass Spectrometry

Deuterium labeling was initiated with an 18-fold dilution into D_2O buffer (10 mM Hepes pD 7.0, 150 mM NaCl) of a pre-equilibrated (30 min, RT) aliquot of each protein, protein:ligand, peptide, and peptide:ligand stock solution. At the indicated time points, the labeling reaction was quenched with the addition of an equal volume of quench buffer (150 mM potassium phosphate, pH 2.54). Protein and protein:ligand exchange

reactions were directed to local exchange analysis while peptide and peptide:ligand exchange reactions were directed to global exchange analysis. For global exchange mass analysis, samples were injected onto a POROS 20 R2 protein trap immediately after quenching the labeling reaction, and then desalted with 0.05% trifluoroacetic acid (TFA) in water at a flow rate of 500 μL/min. The proteins were eluted into the mass spectrometer using a 15-75% linear gradient of acetonitrile over 4 min at 50 μL/min with a Shimadzu HPLC system (LC-20AD). Mass spectral analyses were carried out using a Waters LCT-Premier^{XE} mass spectrometer. Relative deuterium levels for each peptide were calculated by subtracting the average mass of the undeuterated control sample from that of the deuterium labeled sample. For local exchange mass analysis, samples were injected immediately after the quench reaction into a nanoACQUITY with HDX technology(Wales et al., 2008) for online pepsin digestion using a 2.1 mm x 30 mm Poroszyme® immobilized pepsin cartridge (Life Technologies™). The peptides were trapped and desalted on a VanGuard Pre-Column trap (2.1 x 5 mm, ACQUITY UPLC BEH C18, 1.7 μm) for 3 min, eluted from the trap using a 5-35% gradient of acetonitrile over 6 min at a flow rate of 60 μL/min, and then separated using an ACQUITY UPLC HSS T3, 1.8 μm, 1.0 x 50 mm column. Peptides from an unlabeled protein were identified in triplicate using ProteinLynx Global Server (PLGS) searches of a protein database including analyte protein and ligands, as well as porcine pepsin A1(Wales et al., 2013). All mass spectra were acquired using a Waters SYNAPT G2 mass spectrometer. Each deuterium labeling experiment was performed in duplicate. The error of determining the average deuterium incorporation for each peptide was at or below +/- 0.25 Da. Relative deuterium levels for each peptide were calculated by subtracting the average mass of the undeuterated control sample from that of the deuterium-labeled sample. All mass spectra were processed using DynamX 2.0 supplied from Waters. Deuterium levels were not corrected for back exchange and are therefore reported as relative(Wales and Engen, 2006).

NMR Sample Preparation and Spectroscopy

Uniformly ^{15}N-labeled full-length human BAX was generated as previously described(Gavathiotis et al., 2008). BCL-2 BH4 SAHBs (10 mM stock) were added to a solution of 50 μM BAX to achieve a 1:1.1 (MTSL-derivatized SAHBs) or 1:2 molar ratio. Samples were prepared in 20 mM potassium phosphate solution at pH 6.0 with 25 mM NaCl and 10% DMSO-d_6. Spectra were acquired at 25 °C on Bruker 800 MHz and 600 MHz NMR spectrometers, processed using Topspin 3.0 and analyzed with CCPNMR 2.3.1(Vranken et al., 2005). The pulse program used to acquire the correlation spectra was ^{1}H-^{15}N HSQC (hsqcetf3gpsi)(Palmer et al., 1991). The weighted average chemical shift perturbation (CSP) at the molar ratio of 1:1.1 or 1:2 was calculated as $\sqrt{(\Delta H)^2+(\Delta N/5)^2}$ in p.p.m. The absence of a bar indicates no chemical shift difference, or the presence of a proline or residue that is overlapped or not assigned. BAX cross-peak assignments were applied as previously reported(Suzuki et al., 2000). The significance threshold for backbone amide chemical shift changes was calculated based on the average chemical shift across all residues plus the standard deviation, in accordance with standard methods(Marintchev et al., 2007).

Structure Calculations

Structure calculations were performed with Crystallography and NMR system solve (CNS) within the HADDOCK web server using the expert interface(de Vries et al., 2010). HADDOCK calculations generated models of the complex that are in agreement with experimental distance restraints and have optimal electrostatic and van der Waals interactions based on a combination of molecular dynamics and energy minimization. HADDOCK docks were performed using the BAX NMR structural ensemble imported directly from the PDB (PDB ID: 1F16); three constructs of the BCL-2 BH4 helix were used in the docking protocol; residues 13 to 32 were taken from both the BCL-2 NMR and X-ray structures (PDB ID: 2O22 and 4IEH) and in both cases gaps were filled in and the structure minimized using the Molecular Operating Environment (MOE 2013.0802, Chemical Computing Group Inc., Canada); and a third structure of the BCL-2 BH4 as a continuous helix was generated using MOE. Structures generated from the native-like BH4-structures from the BCL-2 PDB structures gave generally higher energy structures with less agreement to the NMR data. Therefore, all final docking solutions originated from runs using the all-helical structure. The wild-type sequence was employed for all docking runs. Calculations were performed with ambiguous interaction restraints (AIR) derived from the chemical shift perturbations, with and without PRE-based interaction restraints. In both cases, the BCL-2 BH4 peptide was localized to the same binding site based on the lowest energy and most populous clusters. For BAX AIR calculations, only residues that exhibited significant chemical shift upon titration and solvent accessibility over 50% as determined by the program NACCESS(Hubbard and Thornton, 1993) were defined as active residues; passive residues were automatically assigned by the HADDOCK web interface. For BCL-2 BH4, AIR restraints were assigned based on functional mutation data; residues reducing BH4-mediated inhibition of liposomal release by 50% or more were defined as active while those inhibiting by 20-50% were defined as passive residues. Active residues for BAX included residues 36, 37, 38, 39, 40, 41, 42, 82, 84, 85, 123, 126, 127, 128, and 129; active residues for BCL-2 BH4 were defined as 17, 18, 19, 23, 27 and 28. PRE-derived distance restraints defined any residue with Iox/Ired values <0.7 as a distance restraint of no more than 25 Å from the back bone amide to the CB atom of the residue containing the MTSL spin label. For each restraint set, 1000 orientations/structures of the complex were generated by rigid-body docking energy minimization of the individual structures. The 200 lowest energy structures were semi-flexibly refined in torsion angle space and then refined in explicit solvent. Structures formed a cluster within a 7.5 Å cut-off.
Ribbon diagrams and molecular models were depicted using PYMOL.

Supplemental References

Bird, G.H., Bernal, F., Pitter, K., and Walensky, L.D. (2008). Synthesis and biophysical characterization of stabilized alpha-helices of BCL-2 domains. Methods in enzymology *446*, 369-386.

de Vries, S.J., van Dijk, M., and Bonvin, A.M. (2010). The HADDOCK web server for data-driven biomolecular docking. Nature protocols *5*, 883-897.

Gavathiotis, E., Suzuki, M., Davis, M.L., Pitter, K., Bird, G.H., Katz, S.G., Tu, H.-C., Kim, H., Cheng, E.H.-Y., Tjandra, N.*, et al.* (2008). BAX activation is initiated at a novel interaction site. Nature *455*, 1076-1081.

Hubbard, S.J., and Thornton, J.M. (1993). NACCESS. University College London.
Marintchev, A., Frueh, D., and Wagner, G. (2007). NMR methods for studying protein-protein interactions involved in translation initiation. Methods in enzymology *430*, 283-331.

Palmer, A.G., Cavanagh, J., Wright, P.E., and Rance, M. (1991). Sensitivity improvement in proton-detected 2-dimensional heteronuclear correlation NMR spectroscopy. J Magn Reson *93*, 151-170.

Suzuki, M., Youle, R.J., and Tjandra, N. (2000). Structure of Bax: coregulation of dimer formation and intracellular localization. Cell *103*, 645-654.

Vranken, W.F., Boucher, W., Stevens, T.J., Fogh, R.H., Pajon, A., Llinas, M., Ulrich, E.L., Markley, J.L., Ionides, J., and Laue, E.D. (2005). The CCPN data model for NMR spectroscopy: development of a software pipeline. Proteins *59*, 687-696.

Wales, T.E., Eggertson, M.J., and Engen, J.R. (2013). Considerations in the analysis of hydrogen exchange mass spectrometry data. Methods Mol Biol *1007*, 263-288.

Wales, T.E., and Engen, J.R. (2006). Hydrogen exchange mass spectrometry for the analysis of protein dynamics. Mass spectrometry reviews *25*, 158-170.

Wales, T.E., Fadgen, K.E., Gerhardt, G.C., and Engen, J.R. (2008). High-speed and high-resolution UPLC separation at zero degrees Celsius. Anal Chem *80*, 6815-6820.